

Single-Shot Pose Estimation of Surgical Robot Instruments' Shafts from Monocular Endoscopic Images

Masakazu Yoshimura, Murilo M. Marinho, Kanako Harada, Mamoru Mitsuishi

Abstract—Surgical robots are used to perform minimally invasive surgery and alleviate much of the burden imposed on surgeons. Our group has developed a surgical robot to aid in the removal of tumors at the base of the skull via access through the nostrils. To avoid injuring the patients, a collision-avoidance algorithm that depends on having an accurate model for the poses of the instruments' shafts is used. Given that the model's parameters can change over time owing to interactions between instruments and other disturbances, the online estimation of the poses of the instrument's shaft is essential. In this work, we propose a new method to estimate the pose of the surgical instruments' shafts using a monocular endoscope. Our method is based on the use of an automatically annotated training dataset and an improved pose-estimation deep-learning architecture. In preliminary experiments, we show that our method can surpass state of the art vision-based marker-less pose estimation techniques (providing an error decrease of 55% in position estimation, 64% in pitch, and 69% in yaw) by using artificial images.

I. INTRODUCTION

Robot-assisted surgery has many advantages over manual surgery. In robot-assisted surgery, surgeons' hand tremors are filtered, and they can move robotic instruments more precisely. Moreover, surgeons can efficiently perform dexterous manipulation of robotic instruments that have multiple degrees of freedom at the tip, whereas hand-held surgical instruments have limited dexterity. Considering these advantages, we are developing a versatile robot, called SmartArm [1], designed with a focus on procedures in deep and narrow spaces.

One of the applications of the SmartArm is endonasal surgery, in which transsphenoidal surgery is one goal. Transsphenoidal surgery is a procedure to remove tumors of the pituitary gland or other tumors at the skull base, as shown in Fig. 1. In robot-assisted surgeries in constrained workspaces such as the nasal cavity, surgeons have restricted vision to the region near the surgical instruments' tips. To autonomously prevent collisions between the robots and surrounding tissues, we have developed a virtual-fixtures framework based on the kinematic model of the robots [2].

However, even with the careful offline calibration of the robots' parameters and in a considerably controlled environment, we can still observe a mismatch of a few millimeters between the kinematic model and the absolute pose¹ of

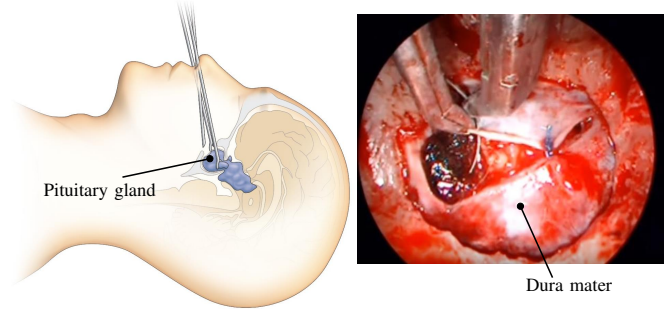


Fig. 1. Transsphenoidal surgery (left) and the endoscopic image during dura mater suturing (right).

the tools. Moreover, even if a perfect offline calibration of the robots were possible, disturbances such as changes in temperature and the interactions of the tools with tissues cause the robots' parameters to change over time. This mismatch between the calculated pose and the absolute pose of the robots' instruments are even more pronounced in cable-driven robots, as reported in related literature [3], [4] using the da Vinci Surgical System (Intuitive Surgical, USA), which is a robotic system routinely used for surgeries *in-vivo*.

The reason why this mismatch is not apparent for users in teleoperation [5] is that the human operator “closes the loop” by using their vision. As we move towards (semi-)automation of surgical tasks, a system to “close the loop” and provide online calibration of the tool parameters is paramount. Moreover, it is important to achieve a highly-accurate parameter calibration given that the effectiveness of the collision avoidance depends heavily on the accuracy of the robots' model.

A. Related works

Many strategies have been proposed to estimate the pose of surgical instruments. Some require added sensors, such as ultrasound [6] or electromagnetic trackers [7]. Such a requirement makes it difficult to impact existing operating rooms, and the sensors themselves have limitations that should be considered. For instance, the propagation of ultrasound is affected by its medium, and electromagnetic sensors are affected by surrounding metallic materials and magnetic fields.

An alternative is to use a stereo camera. Allan *et al.* [8] calculated the pose of surgical instruments from the parallax of a stereo laparoscope using a particle filter and optical flow after semantic segmentation. Other approaches, based on correlating the 2D images to 3D templates. Baek *et al.* [9]

This work was supported by JSPS KAKENHI Grant Number 19K14935. (Corresponding author: Murilo M. Marinho)

Masakazu Yoshimura, Murilo M. Marinho, Kanako Harada, and Mamoru Mitsuishi are with the Department of Mechanical Engineering, the University of Tokyo, Tokyo, Japan. Emails: {m.yoshimura, murilo, kanako, mamoru}@nml.t.u-tokyo.ac.jp.

¹Pose means combined position and orientation.

used particle filtering and kinematic data to track instruments of a microsurgical robotic system. Moccia *et al.* [4] used feature matching and an extended Kalman filter to estimate and track the pose of the da Vinci’s instruments. However, endonasal procedures require thin (3 mm) endoscopes, that are not currently available on the market.

Printable markers have been proposed by Gadwe *et al.* [10], but that would also require modifying the surgical instruments.

Based on the above, we aim to estimate the instruments’ pose with a monocular endoscope. A myriad of works have explored the estimation of instruments’ pose from monocular images. For example, Reiter *et al.* [3] estimated the da Vinci’s instruments’ pose using keypoint information. Ye *et al.* [11] studied keypoint extraction and parts-based template matching to estimate tool pose even in occluded situations. Zhou and Payandeh [12] estimated the pose from the position of straight contour lines and the tip on the image. Other groups [13], [14] have proposed the estimation by two-step approaches, using the segmentation and template matching method plus object tracking. In this category of instrument pose estimation, errors larger than 2.8 mm in position and 4.8° in rotation are reported. Accurate pose estimation of surgical instruments from monocular images is still a challenging task.

Deep learning technology is being rapidly developed and pose estimation of objects from monocular images with end-to-end learning and inference has been studied in the past few years. For example, Sundermeyer *et al.* [15] estimated the pose of real objects from monocular images using a training dataset composed of artificial images rendered from 3D simulated objects. In their approach, the objects are first detected using single-shot detection (SSD) [16]; then, the pose is estimated using an auto-encoder trained with artificial images. In another work, Kehl *et al.* [17] proposed the SSD-6D method, in which the object pose was estimated directly as the output of the SSD together with the bounding boxes of objects on the images. To the best of our knowledge, these methods have not been applied to the pose estimation of surgical tools.

B. Limitations of current methods

In a pilot evaluation, we attempted to use the SSD-6D methodology directly to estimate the pose of the shaft of our surgical instruments in our robotic setup. We identified two limitations of the current methods that we address in this work:

- 1) In SSD-6D, the pose estimation is regarded as a classification problem by discretizing the pose-space. For example, rotations were classified in five-degree steps, that are not precise enough for the pose estimation of surgical instruments.
- 2) It is assumed that the objects are reasonably far from the camera, so the images are mostly unaffected by perspective distortions. This assumption does not hold true in the case of endonasal endoscopic images because the instruments are close to the lens, and endoscopes

usually have wide perspective angles. This causes the object’s shape to be deformed in the endoscopic image owing to perspective distortions (closer parts of the object look larger than farther parts of the same object).

C. Statement of contributions

With prior literature in mind, our goal in this work is to estimate the pose of surgical instruments from monocular endoscopic images using deep learning end-to-end. Our use-case breaks some of the assumptions of earlier methods because the appearance of the instrument’ changes according to the distance from the endoscope due to perspective distortions. Moreover, only the tips of the instruments can be seen on endoscopic images. To overcome these issues, we propose a new deep learning architecture. It is an improved architecture of the SSD-6D [17] that performs regression instead of classification. The network also responds well to occlusion and a varying number of instruments. The generation of training data also relies partially on artificial data augmentation, using computer graphics (CG) rendering software. Our results show that we can accurately estimate the pose of surgical instruments from real endoscopic images. To the best of our knowledge, the accuracy of our method is the state of the art in vision-based and marker-less pose estimation of surgical instruments.

II. PROBLEM STATEMENT

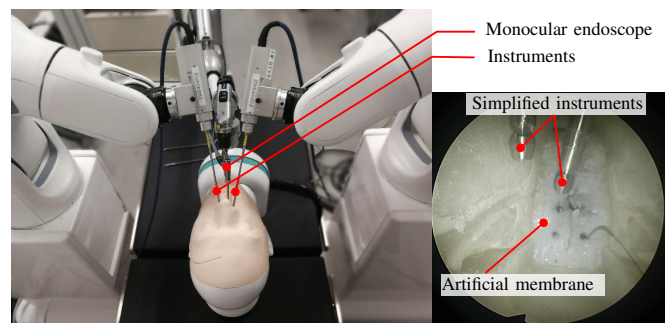


Fig. 2. Robot setup (left) and its inner view from a 70° endoscope (right).

Given the robot-aided endonasal surgery setup, as shown in Fig. 2, let there be two robotic arms (SmartArm [1]) with instruments as their end effectors. Those instruments are inserted through the nostrils of an anatomically-realistic head model (BionicBrain [18]). Images are obtained through a high-definition endoscopic system (Endoarm, Olympus, Japan) with a 70° endoscope with perspective angle of 95°.

For this work, suppose that we are only interested in finding the pose of the instrument’s shaft because this information is enough for appropriate collision avoidance in the context of endonasal surgery [2]. The reference frames of the instruments are attached to their distal tip, and the z -axis is along the instruments’ shaft. In this context, our target is to estimate the pose of the instruments’ shafts relative to the monocular endoscope. In future work, our vision will be feedback this information to the robot controller, to adapt the

robot’s parameters, and to increase the safety and precision of the robot-aided procedure.

III. METHODOLOGY

This paper proposes a new method of pose estimation of the surgical instrument’s shafts from monocular endoscopic images. In this section, we first describe how to create a training dataset composed of artificial CG images. Second, we explain our proposed network architecture for pose estimation. Lastly, we explain the data augmentation approach and the loss function.

A. Training dataset

Deep convolutional neural networks (DCNNs) are known to need a large amount of training data to avoid over-fitting, and manual annotation is a time-consuming and error-prone task. In multi-task learning, even more complicated annotation is required. For instance, in SSD-6D and this work, the semantic annotation, the bounding boxes, and the precise pose of the shafts are necessary. To address this issue, we partially relied on the automatic annotation of CG images using an open-source rendering software (Blender, Blender Foundation, Netherlands), using a rendering pipeline based on [19].

To generate the CG images, real endoscopic images of the realistic head-model were used as the background. To prevent over-fitting to the background images, more background images were generated by altering the hue, saturation, and brightness of the original background images. The intensity of the light coming from the virtual endoscope was also varied to increase the amount of data. Robotic instruments are metallic; therefore, they have a considerable specular reflection. To correctly render background reflections in the shafts, the background images were replicated in a cubic region around the shafts. The shafts themselves are artificially rendered from a CAD model using physics-based shaders. The surface roughness of the shafts was rendered using a normal map.

The shafts were rendered in random poses that are possible in endonasal surgery. In detail, the poses were randomly chosen from the ranges displayed in Table. I. The rotation about the shaft was excluded because of the rotational symmetry. We created 100000 images in total. Some examples of artificially generated images are shown in Fig. 3. The rendering software automatically generates realistic CG images together with appropriate bounding box information.

TABLE I

RANGE FOR THE GENERATION OF THE AUTOMATICALLY ANNOTATED DATA.

Dimension	x [mm]	y [mm]	z [mm]	pitch [degree]	yaw [degree]
Range	-20~20	-20~20	10~40	50~90	0~358

B. Additional Training Methodologies

The deep neural networks proposed in the next section have a limited capability of generalizing from purely artificial images to real images. However, it is difficult to obtain the precise pose of the instruments in a real setup.

To balance this, we added to our dataset some real endoscopic images and the manual annotation of their bounding boxes. For now, no pose information was added to the real images. There is an ongoing research effort in our group to create such a real dataset.

C. Network architecture

1) *Backbone network*: Our network can be regarded as an extension of the SSD-6D network [17]. We use a network created by extending the InceptionV4 [20] as the backbone of the SSD [16]. The padding of 'Inception-B' is changed to obtain odd size feature maps.

The input of the network is a $299 \times 299 \times 3$ (width \times height \times color) image, resized from the high-definition images obtained from the endoscope. Different from SSD-6D, our backbone network reduces the image to 2×2 feature maps instead of using 71×71 feature maps. This was changed so that our network could appropriately detect the shafts, given that they occupy a large portion of the image. The backbone network is detailed in Fig. 4, and its outputs are six feature maps that are fed to the SSD-like network.

2) *Detection and pose estimation network*: In this work, we explore two architectures for instrument detection and pose estimation. The first architecture is the naive adjustment of the SSD-6D [17] network to perform regression, as shown in Fig. 4 (b). The other architecture is a more intricate network that feeds the class confidence prediction output and bounding box prediction output to the pose estimation path to increase the quality of the pose estimation, as shown in Fig. 4 (c). We added ReLU activations and batch normalization to improve the backpropagation. The concatenation of the bounding box prediction path to the pose estimation path aims to give information on whether the instruments are in the region. This facilitates the network learning in that it outputs a valid pose value if the instruments are in the region or outputs zero if the instruments are not in the region.

The networks output pose estimation maps, bounding box maps, and class confidence maps. The bounding box maps and class confidence maps are unchanged from SSD. The pose estimation outputs are normalized to $[-1, 1]$, and the outputs are set to 0 if the instruments are not on that location.

The shape of the output of the network is $(w_i, h_i, (C + 4 + P)N_i)$ per feature map $i = 1, 2, 3, 4, 5, 6$ of the backbone network. The size of each output is the same as the matching input feature map (w_i, h_i) , and N_i is the number of bounding boxes per location that have different aspect ratios. There is a pose estimation for each bounding box (w_i, h_i, P) , an estimation of the parameters of the bounding box itself $(w_i, h_i, 4)$, and an estimation of the class confidence (w_i, h_i, C) . Lastly, $P = 5$ is the number of pose

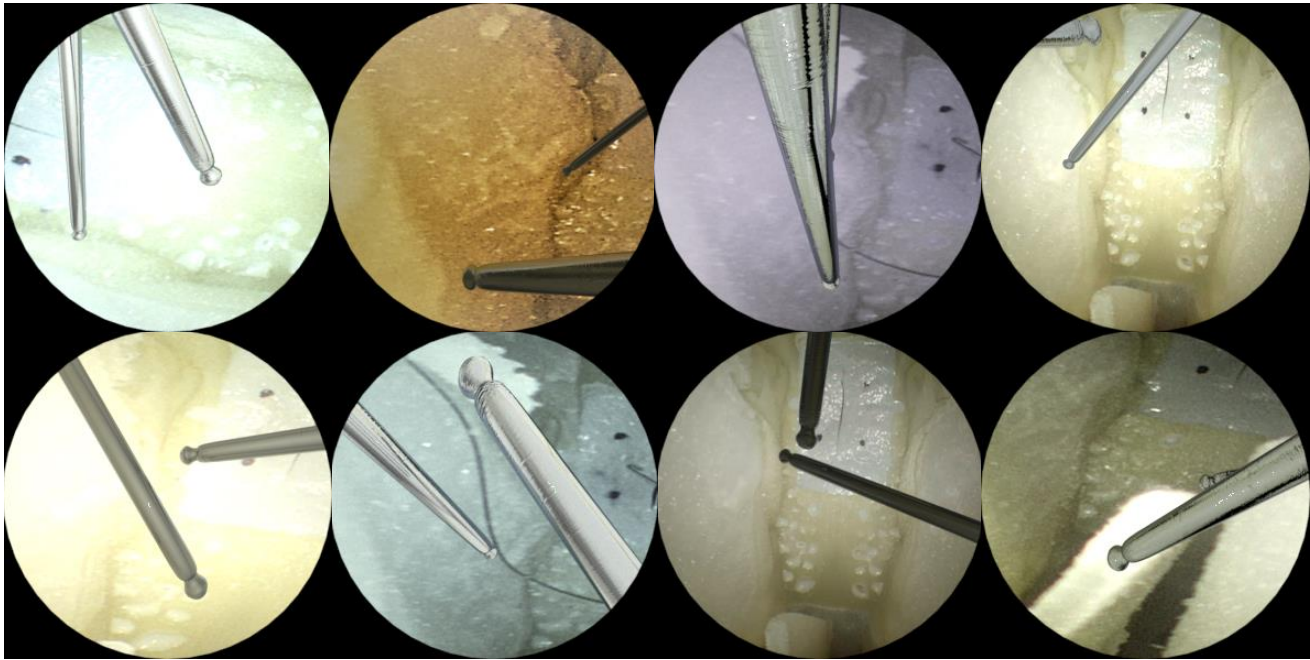


Fig. 3. Samples of artificial images.

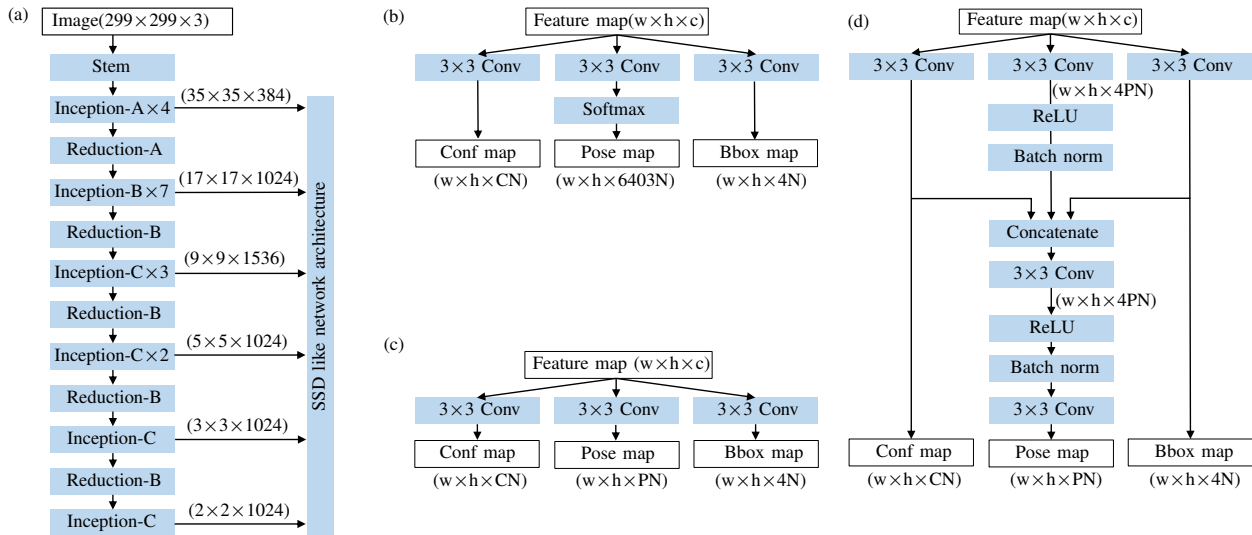


Fig. 4. The proposed network architecture. (a) is the backbone of the SSD-like network created by extending Inception-V4 network. (b) is the SSD-like architecture proposed in SSD-6D, and the pose output is in one-hot format. (c) and (d) are proposed SSD-like architectures which output class confidence maps, bounding box maps, and pose maps. (c) is the naive adjustment of the SSD-6D [17] network to perform regression. (d) is an improved architecture to estimate the pose more accurately. $P = 5$ is the pose dimension.

dimensions and $C = 2$ is the number of classes (instruments or background).

The detection and pose estimation network outputs many candidates of bounding boxes and their corresponding pose estimation. The top K high probability bounding-box candidates are chosen. Subsequently, the final output of the bounding boxes is chosen using non-maximum suppression. The final pose estimation is the pose corresponding to the bounding boxes output by the non-maximum suppression.

D. Data augmentation

At the training stage, several data augmentation methods are used. For example, brightness, saturation, hue, and contrast of images are randomly changed. Random additive noise is also added to each pixel of each channel on some input images to increase the network's robustness to different textures.

E. Loss function

Our loss functions were defined as

$$L = \frac{1}{n} (L_{conf} + \alpha L_{bbox} + L_{pose})$$

where n is the number of matched anchors. If the number of matched anchors is 0, we set n as 1. L_{conf} is a softmax cross-entropy loss for the class confidence map. We used the hard negative mining method in L_{conf} whose ratio between the negatives and the positives is 3:1, similar to SSD [16]. L_{bbox} is a smooth L1 loss for the bounding box estimation map. L_{pose} is defined as

$$L_{pose} = \sum_p \beta_p L_1 (\gamma (X_p^{pred} - X_p^{target}))$$

where p denotes the pose dimension and L_1 is a smooth L1 loss function. X_p^{pred} and X_p^{target} are the pose estimation and the correct pose of dimension p . α , β_i , and γ are weighting parameters.

The Adam optimizer and a polynomial decay learning rate with power 2.0 were used for the smooth convergence of the loss.

1) Loss switching for the training with real images:

Whenever the network was trained using real images, we assigned 0 to L_{pose} . This was required because the real images did not have pose annotations.

IV. EVALUATION

Two experiments were conducted to evaluate our method. In the first experiment, the quality of the pose estimation was evaluated on artificial images. In the second experiment, we evaluated the proposed network on real endoscopic images.

The same parameters were used for all architectures. Ninety thousand artificial images were used as training data, and another 10000 images were used as test data. The parameters were $\alpha = 1.5$, $\gamma = 5.0$, $\beta_i = (1.0, 1.0, 2.0, 2.0, 2.0)$ in the order of (x, y, z, pitch, yaw) making the weights larger in the dimensions that are difficult to estimate from monocular images. Moreover, we used a batch size of 32 during the training stage, and the detection threshold of the SSD-like architecture was set to 0.5 IoU both in training and test stages. The anchor ratio was the same as in SSD. The top 250 probability detected candidates were chosen and they were input in the non-maximum suppression. All the architectures were implemented in Python 3.6 using TensorFlow 1.13 and cuDNN 7.4 and executed in Ubuntu 18.04 with a Quadro GV 100 graphics card.

A. Evaluation on artificial images

We first evaluated the error of the pose estimation using 10000 artificial test images. We compared the performance of the naive adjustment of SSD-6D, which we call Architecture-C, with the proposed architecture that we call Architecture-D. Architecture-C and Architecture-D denote the networks using (c) and (d) of Fig. 4, respectively.

The evaluation metrics were the mean average precision (mAP), detection rate, and pose error. The mAP was used as defined in PASCAL VOC 2010 [21]. For the detection rate calculation, the instrument was considered detected even

if that single instrument was detected as two instruments. Lastly, we evaluated the average pose error.

The results of the evaluation of the two architectures are shown in Table. II. Our results showed a considerable increase in the quality of the estimation between Architecture-C (prior method) and Architecture-D (proposed method). There were decreases of 50% , 45% , and 63% in the translation error, the pitch estimation error, and the yaw estimation error, respectively.

To further improve the results of Architecture-D, we added uniform random noise [-10.0, 10.0] to each pixel of each channel on a training image with a 50% probability. The result was 'D with noise' Table. II, which improved the pose estimation.

To allow the network to generalize well to real images, we added 100 real images with manual bounding box annotation. We fed a mixture of real images and artificial images to the network with a ratio of 2:9. The random uniform noise was also added. The result was 'D with noise and real' in Table. II. The detected rate and pose estimation accuracy did not decrease in artificial images even though the real images did not have any pose information.

To conclude this evaluation, Architecture-D ran on 30.4 fps which is suitable for our real-time robot control. Comparing the best training strategy of Architecture-D with the naive adjustment of SSD-6D (Architecture-C), there was an error decrease of 55% in position estimation, 64% in pitch, and 69% in yaw.

TABLE II
EVALUATION RESULTS ON ARTIFICIAL TEST IMAGES.

	mAP	Detected rate	Pose error				
			x [mm]	y [mm]	z [mm]	pitch [degree]	yaw [degree]
Architecture-C (prior method)	0.958	0.937	1.51	1.41	1.64	3.97	13.58
Architecture-D (proposed method)	0.949	0.956	0.81	0.76	0.81	1.57	5.30
D with noise	0.965	0.985	0.65	0.63	0.75	1.44	4.26
D with noise and real	0.965	0.988	0.66	0.64	0.77	1.44	4.33

'D with noise' means the result of Architecture-D using random noise data augmentation and 'D with noise and real' means the result of Architecture-D using the random noise and real data.

B. Preliminary evaluation on real images

In the former experiment, the accuracy of the detection and pose estimation were validated on artificial images and their automatic annotation. In this section, an experiment was performed to evaluate the performance of the 'D with noise' network and the 'D with noise and real' network on real endoscopic images. However, given that we did not have a dataset with the pose of real instruments, we evaluated the detected rate and intersection over union (IoU).

To do so, first, we estimated the pose of the instruments in the real images using the proposed network; then, we rendered artificial tools on Blender using this pose information to generate the semantic segmentation of the tools. We could then compare the estimated semantic segmentation with manually annotated images to obtain the IoU. In total,

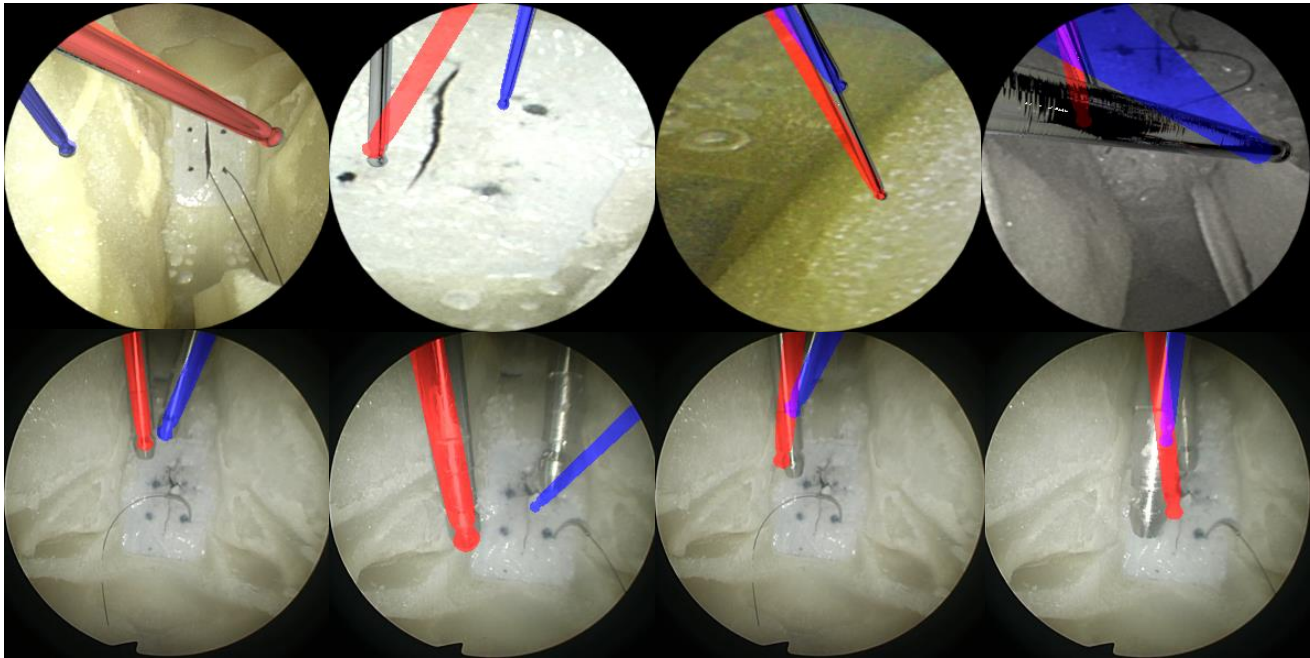


Fig. 5. Visualization of the estimated pose. The upper images are artificial images and the lower ones are real endoscopic images.

40 real endoscopic images were evaluated; 20 of them had no occlusion and the others had heavily occluded instruments.

The result of this evaluation is shown in Table. III and Fig. 5. It is important to note that the absolute value of the IoU, in this case, is not always a good indicator of pose error, as shown in Table. II. Nonetheless, the relative value of the IoU evaluated on real images with respect to the IoU evaluated on artificial images shows that the method can also be applied to real images to some extent. This result is interesting because there was no pose annotation for the real images used during the training of the network and the network still learned how to estimate the instrument’s pose. There is an ongoing effort in our group to improve the quality of our dataset to include real images with full annotation.

TABLE III

PERFORMANCE COMPARISON OVER ARTIFICIAL IMAGES AND REAL ENDOSCOPIC IMAGES.

		non occluded images		partly occluded images	
		Detected rate	IoU	Detected rate	IoU
Artificial	D with noise and real	0.950	0.494	0.850	0.369
Real	D with noise	0.700	0.197	0.700	0.195
	D with noise and real	0.950	0.471	0.825	0.299

V. CONCLUSIONS

In this paper, we proposed a deep-learning methodology to estimate the pose of the shaft of surgical instruments in monocular endoscopic images. To do so, we extended the SSD-6D [17] network. We also created a dataset composed of artificially rendered images with the automatic annotation of the instruments’ bounding boxes and poses.

In the context of our study, we could considerably decrease pose estimation error (55% in position estimation, 64% in pitch, and 69% in yaw) with our proposed architecture in an experiment using artificial images. Moreover, in a preliminary experiment using real images, we showed that the network could generalize from real images to some extent. Further work must be done to improve our training dataset and add real images with pose annotation.

This is an important first step in our goal to the online calibration of the instrument’s shafts, aiming at reliable collision avoidance for robot-aided surgical procedures in constrained workspaces. Our method should be applicable for other instrument designs as long as the instrument has a prominent shaft. In future works, we intend to utilize sequential video information to increase the robustness of our predictions.

REFERENCES

- [1] M. M. Marinho, K. Harada, A. Morita, and M. Mitsuishi, “SmartArm: Integration and validation of a versatile surgical robotic system for constrained workspaces,” *The International Journal of Medical Robotics and Computer Assisted Surgery*, 2020, (in press).
- [2] M. M. Marinho, B. V. Adorno, K. Harada, and M. Mitsuishi, “Dynamic active constraints for surgical robots using vector-field inequalities,” *IEEE Transactions on Robotics*, vol. 35, no. 5, pp. 1166–1185, oct 2019.
- [3] A. Reiter, P. K. Allen, and T. Zhao, “Appearance learning for 3d tracking of robotic surgical tools,” *The International Journal of Robotics Research*, vol. 33, no. 2, pp. 342–356, 2014.
- [4] R. Moccia, C. Iacono, B. Siciliano, and F. Ficuciello, “Vision-based dynamic virtual fixtures for tools collision avoidance in robotic surgery,” *IEEE Robotics and Automation Letters*, vol. 5, no. 2, pp. 1650–1655, apr 2020.
- [5] M. M. Marinho, B. V. Adorno, K. Harada, K. Deie, A. Deguet, P. Kazanzides, R. H. Taylor, and M. Mitsuishi, “A unified framework for the teleoperation of surgical robots in constrained workspaces,” in *2019 International Conference on Robotics and Automation (ICRA)*. IEEE, may 2019, pp. 2721–2727.

- [6] H. Ren and P. E. Dupont, "Tubular enhanced geodesic active contours for continuum robot detection using 3d ultrasound," in *2012 IEEE International Conference on Robotics and Automation*. IEEE, 2012, pp. 2907–2912.
- [7] C. Kim, S. C. Ryu, and P. E. Dupont, "Real-time adaptive kinematic model estimation of concentric tube robots," in *2015 IEEE/RSJ International Conference on Intelligent Robots and Systems (IROS)*. IEEE, 2015, pp. 3214–3219.
- [8] M. Allan, P.-L. Chang, S. Ourselin, D. J. Hawkes, A. Sridhar, J. Kelly, and D. Stoyanov, "Image based surgical instrument pose estimation with multi-class labelling and optical flow," in *International Conference on Medical Image Computing and Computer-Assisted Intervention*. Springer, 2015, pp. 331–338.
- [9] Y. M. Baek, S. Tanaka, K. Harada, N. Sugita, A. Morita, S. Sora, and M. Mitsuishi, "Robust visual tracking of robotic forceps under a microscope using kinematic data fusion," *IEEE/ASME Transactions on Mechatronics*, vol. 19, no. 1, pp. 278–288, feb 2014.
- [10] A. Gadwe and H. Ren, "Real-time 6dof pose estimation of endoscopic instruments using printable markers," *IEEE Sensors Journal*, vol. 19, no. 6, pp. 2338–2346, 2018.
- [11] M. Ye, L. Zhang, S. Giannarou, and G.-Z. Yang, "Real-time 3d tracking of articulated tools for robotic surgery," in *International Conference on Medical Image Computing and Computer-Assisted Intervention*. Springer, 2016, pp. 386–394.
- [12] J. Zhou and S. Payandeh, "Visual tracking of laparoscopic instruments," *Journal of Automation and Control Engineering*, vol. 2, no. 3, pp. 234–241, 2014.
- [13] R. Hao, O. Özgüner, and M. C. Çavuşoğlu, "Vision-based surgical tool pose estimation for the da vinci® robotic surgical system," in *2018 IEEE/RSJ International Conference on Intelligent Robots and Systems (IROS)*. IEEE, 2018, pp. 1298–1305.
- [14] M. Allan, S. Ourselin, D. J. Hawkes, J. D. Kelly, and D. Stoyanov, "3-d pose estimation of articulated instruments in robotic minimally invasive surgery," *IEEE transactions on medical imaging*, vol. 37, no. 5, pp. 1204–1213, 2018.
- [15] M. Sundermeyer, Z.-C. Marton, M. Durner, M. Brucker, and R. Triebel, "Implicit 3d orientation learning for 6d object detection from rgb images," in *Proceedings of the European Conference on Computer Vision (ECCV)*, 2018, pp. 699–715.
- [16] W. Liu, D. Anguelov, D. Erhan, C. Szegedy, S. Reed, C.-Y. Fu, and A. C. Berg, "Ssd: Single shot multibox detector," in *European conference on computer vision*. Springer, 2016, pp. 21–37.
- [17] W. Kehl, F. Manhardt, F. Tombari, S. Ilic, and N. Navab, "Ssd-6d: Making rgb-based 3d detection and 6d pose estimation great again," in *Proceedings of the IEEE International Conference on Computer Vision*, 2017, pp. 1521–1529.
- [18] T. Masuda, S. Omata, A. Morita, T. Kin, N. Saito, J. Yamashita, K. Chinzei, A. Hasegawa, T. Fukuda, M. Mitsuishi, K. Harada, S. Adachi, and F. Arai, "Bionic-brain: Training of endoscopic endonasal skull base surgery," in *2019 The Proceedings of JSME annual Conference on Robotics and Mechatronics (Robomec)*. The Japan Society of Mechanical Engineers, jun 2019, pp. 2P2–R08.
- [19] M. M. Marinho, Y. Yatsushima, T. Maekawa, and Y. Namioka, "Preliminary evaluation of a framework for overhead skeleton tracking in factory environments using kinect," in *Proceedings of the 4th international Workshop on Sensor-based Activity Recognition and Interaction - iWOAR17*. ACM Press, 2017.
- [20] C. Szegedy, S. Ioffe, V. Vanhoucke, and A. A. Alemi, "Inception-v4, inception-resnet and the impact of residual connections on learning," in *Thirty-First AAAI Conference on Artificial Intelligence*, 2017.
- [21] M. Everingham, L. Van Gool, C. K. I. Williams, J. Winn, and A. Zisserman, "The PASCAL Visual Object Classes Challenge 2010 (VOC2010) Results," <http://www.pascal-network.org/challenges/VOC/voc2010/workshop/index.html>.